J. Plasma Fusion Res. SERIES, Vol. 4 (2001) 117–123

Experiments and Theory on 2D Electron Vortex Dynamics in Sheared Flows

KABANTSEV Andrey*, DRISCOLL C. Fred, DUBIN Daniel and SCHECTER David[1]
Physics Department, University of California at San Diego, La Jolla, California 92093
[1] *National center for Atmospheric Research, Boulder, Colorado 80307*

(Received: 5 December 2000 / Accepted: 16 August 2001)

Abstract

The motion of self-trapped electron vortices on a background vorticity gradient are studied experimentally, and compared to numerical simulations and analytical theory for 2-dimensional incompressible, inviscid flows. These vortices can be either clumps (vorticity excesses) or holes (vorticity deficits). The vortices mix the background vorticity and tend to level the background gradient. As a result, conservation of momentum dictates that clumps move up the background gradient, whereas holes move down the gradient. The rate of this drift motion is dramatically different for prograde (rotating with the background shear) versus retrograde vortices: a prograde vortex moves at a much slower rate than a retrograde vortex, due to rapid nonlinear mixing of the flow field. We have measured the clump and hole velocities for a wide range of vortex strengths, background gradients, and background shear rates. The measurements are in quantitative agreement with theoretical predictions and numerical simulations. When parameterized by the dimensionless vortex strength ℓ/r_v (where ℓ is the size of the trapped region around the vortex, and r_v is the vortex orbital position, representing a characteristic size of the background streamlines). Experiments also show that the rapidly moving retrograde vortex leaves a spiral density wake, and that instability of this wake eventually generates many long-lived holes, which contribute to the late-time "turbulent" noise.

Keywords:
non-neutral plasma, 2-dimensional flow, rotating fluid, monopolar vortex, vorticity gradient

1. Introduction

The free relaxation of two-dimensional (2D) turbulence has been actively studied for decades, with many applications in astrophysics, geophysics and plasma physics. One relaxation mechanism is viscosity, which causes the bulk kinetic energy of the flow to slowly dissipate. However, 2D flows in plasmas, atmospheres and oceans can rapidly relax to metastable states before viscosity affects the dynamics.

Self-trapped 2D monopolar vortices, immersed in a wide background vorticity distribution, are quite common phenomena in nature and experiments; Jupiter's Great Red Spot, hurricanes and ocean eddies are just some of intriguing examples. A monopolar vortex consists of a patch of fluid rotating around its center, and self-trapped implies the background shear does not destroy it. Generally, both mutual advection and the interaction of vortices with the background vorticity gradient play important roles in 2D hydrodynamics, including various aspects of relaxation toward an ordered state and self-organization of turbulence. In some cases, turbulence relaxes through the migration of vortices to extrema in the background vorticity. Thus,

*Corresponding author's e-mail: akabantsev@ucsd.edu

the vortex/background interaction can cause the vortices to move transverse to the direction of the background flow, either up or down the vorticity gradient. This applies both to magnetized non-neutral plasmas [1-4] and to atmospheric and oceanic turbulence and eddies [5-8]; on geophysical scales, the latitudinal variation of the Coriolis acceleration gives a rotational shear in the background (potential) vorticity gradient, called the *β-effect.*

The prediction of hurricane tracks is a problem of great practical importance, and a lot of theoretical work has been devoted to the subject. Schecter and Dubin recently performed a theoretical analysis of this problem in the specific case when pointlike monopolar vortex of relatively weak strength is placed within a diffuse, circular vortex (background vorticity) [9]. Relatively weak vortex strength means that the size of trapping region in a background flow is much less than a characteristic size of its streamlines. The analysis was focused on cylindrical shear flow, where the flow conserves canonical angular momentum. Conservation of momentum then dictates that positive vortices ("clumps") move up the gradient, whereas negative vortices ("holes") move down the gradient. Generally, the vortex speed is proportional to the background vorticity gradient; however, a vortex that is prograde with respect to the background shear moves about 20 times slower than a retrograde vortex of equal strength. Separate theories were given for the motion of prograde and retrograde vortices. Both theories compare favorably to vortex-in-cell (VIC) simulations and to the experiment.

2. Simple Calculations of Gradient-Driven Drift

We focus on specific case where initial background vorticity $\zeta_b(r,\theta)$ is positive, axisymmetric and monotonically decreasing with radius at $t = 0$ (Fig. 1). We neglect viscosity and consider flows that are governed by the 2D Euler equations:

$$\frac{\partial \zeta}{\partial t} + \vec{v} \cdot \nabla \zeta = 0, \quad \vec{v} = \vec{z} \times \nabla \psi, \quad \nabla^2 \psi = \zeta. \qquad (1)$$

Here, $\vec{v}(r,\theta,t)$ is the velocity field, $\zeta(r,\theta,t) \equiv \vec{z} \cdot \nabla \times \vec{v}$ is vorticity, and $\psi(r,\theta,t)$ is a stream function. The coordinates (r,θ) denote polar radius and angle, and t is time. For analysis, the vorticity is decomposed into vortex (v) and background (b): $\zeta = \zeta_b + \zeta_v$.

As we used it before, the vortices can be classified as either clumps or holes, depending of the sign of their vorticity. In shear flows, in addition, they have to be classified as either prograde or retrograde. A prograde vortex rotates with the local background shear, while rotation in the opposite sense defines retrograde vortices. In presented on Fig. 1 background a clump is retrograde and a hole is prograde.

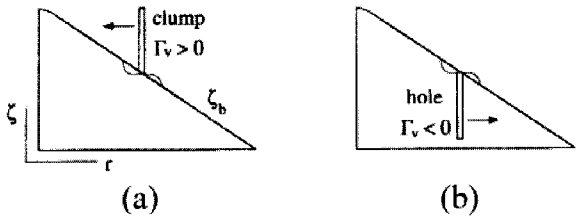

Fig. 1 Schematic representation of an axisymmetric background with either clump (a) or hole (b) on it. Local mixing of the background increases $\langle r^2 \rangle_b$. By conservation of P_θ, clumps and holes react oppositely.

We emphasize here that the conventional terms of cyclones and anticyclones are not adequate to the problem because they can be either clumps or holes, depending on which hemisphere they are located in. Also, prograde or retrograde refers not to the background rotation, but to *the shear* in the background rotation.

The opposite drift of clumps and holes can be easily explained by momentum conservation. Similar arguments have been used to explain the motion of phase-space density clumps and holes in plasma turbulence [10]. We focus on cylindrical geometry, where the flow conserves canonical angular momentum, $P_\theta \equiv \int d^2r \zeta r^2$.

It is convenient to write P_θ in terms of a background contribution and a vortex contribution,

$$P_\theta \equiv \int d^2r r^2 \zeta(r,\theta,t) = \Gamma_b \langle r^2 \rangle_b + \Gamma_v r_v^2. \qquad (2)$$

Here $\Gamma_b > 0$ is total circulation of the background flow, Γ_v is the vortex circulation, r_v is the radial position of the vortex and $\langle r^2 \rangle_b$ denotes the ζ_b-weighted spatial average of r^2. As shown in Fig. 1(a, b), both clumps and holes partially mix the background vorticity and act to level it. As the background is leveled, $\langle r^2 \rangle_b$ increases, since $\partial \zeta_b / \partial r < 0$. To conserve P_θ, the clump ($\Gamma_v > 0$) must decrease r_v and climb the background gradient, whereas the hole ($\Gamma_v < 0$) must increase r_v and descend the gradient.

When there is no local vorticity gradient, local mixing does not affect the background vorticity

distribution. Therefore, where $\partial\zeta_b/\partial r \approx 0$, there is no local mechanism for the vortex to exchange angular momentum or linear momentum with the background. This suggest that clumps will settle on hills of the background vorticity, and that holes will settle in troughs, where $\partial\zeta_b/\partial r = 0$.

We now determine the radial speed of the vortex. Single monopolar vortex consists of a patch of fluid rotating around its common center. The vortex's dominant translational motion is rotation around the center of the background. We work in this rotating frame, so the vortex is nearly stationary, and we defined a local coordinate system centered at the vortex. Figure 2(a, b) shows the initial streamlines in the vicinity of a retrograde clump (a) and a prograde hole (b). The stagnation points in Fig. 2(a) are at distance ℓ above and below the clump, where

$$\ell \equiv \sqrt{\left|\Gamma_v / 2\pi r_v \Omega_0'(r_v)\right|} \qquad (3)$$

is the trapping length, which depends on the clump circulation and on the background shear (here, $\Omega_0(r)$ is the initial rotation frequency of the background).

We treat the vortex and the disturbance that it generates as perturbations to the initial axisymmetric shear flow $\zeta_0(r) \equiv \zeta_b(r, t = 0)$. In case of a weak vortex, with trapping length much less than the streamline size, i.e. $\ell / r_v \ll 1$, it is possible to linearize the Euler equations [Eqs. (1)] to obtain the evolution of the background vorticity perturbation. It is this background perturbation that causes the vortex to leave its initial circular orbit.

Using an unperturbed orbit approximation, after a standard (but lengthy) calculations, Schecter and Dubin have shown [9] that for sufficiently weak vortices the time asymptotic radial drift of the vortex center is approximately given by

$$\frac{dr_v}{dt} = \pm \frac{\pi}{2} \zeta_0' \ell^2 \ln(c \cdot r_v / \ell). \qquad (4)$$

Here, '+/–' is for clumps/holes, and c is a factor of order 1, determined by r_v and the form of $\zeta_0(r)$.

However, by comparing this analytical prediction with results of VIC simulations [9], Schecter and Dubin have found that the linear equations of motion apply only to retrograde vortices, and that nonlinear effects must be kept to explain the slower drift of prograde vortices.

Linear theory breaks down when the trapped fluid becomes mixed over a length scale greater than the

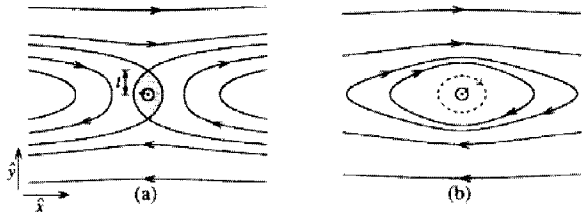

Fig. 2 A sketch of initial streamlines in the vicinity of a retrograde clump (a) and a prograde hole (b) in a shear flow $\Omega_0' < 0$. The center of a circular background flow locates far above the drawings.

trapping length ℓ, which serves as a small length-scale cut-off. Thus, the linear theory breaks down for times greater than the orbital period of a fluid particle located initially at distance $\geq \ell$ from the vortex center. For a retrograde vortex [Fig. 2(a)], the fluid particle is in the outer trapping region, and its angular velocity $|\Omega_0'| \ell$ (in the rotating frame) tends to zero for small vortex circulation; whereas the length of the trapped orbit tends to a finite value of $4\pi r_v$. Thus, for retrograde vortex, the orbital period diverges to infinity as the vortex strength goes to zero. For prograde vortex [Fig. 2(b)], the fluid particle has an orbit of length of $2\pi\ell$ and orbital velocity that is also proportional to ℓ; therefore the orbital period remains constant as the vortex strength goes down. Thus, the time scale for the linear theory to fail becomes "instantaneous" relative to the time scale of vortex motion.

However, a workable estimate of the radial drift velocity of prograde vortex can be obtained using simple "mix-and-move" analysis; here the prograde vortex substantially flattens the mixing layer, and moves a distance determined by conservation of angular momentum during the time needed to flatten the mixing layer. Suppose that the vortex levels the entire mixing layer and has a negligible effect on fluid outside the mixing layer. This mixing increases the background component of P_θ by an amount

$$\Delta P_{\theta,b} \approx -4\pi \zeta_0' r_v^2 \ell^3. \qquad (5)$$

By conservation of P_θ, the hole must increase r_v by an amount Δr. Assuming that $\Delta r / r_v \ll 1$, we have

$$\Delta r = \frac{-\Delta P_{\theta,b}}{2\Gamma_v r_v} \approx \ell \frac{\zeta_0'}{\Omega_0'}. \qquad (6)$$

To obtain the hole velocity, we also require an estimate of the time Δt for the mixing layer to flatten. Presumably, this time is given by the orbital period of a fluid element near the separatrix that encloses the

mixing layer. Since the angular speed of this fluid element is $|\Omega_0'|\,\ell$ (in the rotating frame), and the orbit covers 4π radians (2π in both directions), we have

$$\Delta t \approx \frac{4\pi}{\left|\Omega_0'\right|\,\ell}\,. \tag{7}$$

Finally, the velocity of the prograde vortex is given by

$$\frac{\mathrm{d}r_v}{\mathrm{d}t} \approx \frac{\Delta r}{\Delta t} \approx -\frac{1}{4\pi}\,\ell^2\,\zeta_0'\,. \tag{8}$$

Note that the ℓ-scaling in linear theory [Eq. (4)] differs from the ℓ-scaling in Eq. (8) by a factor of $\ln(c\cdot r_v/\ell)$. Therefore, our estimate suggests that a retrograde vortex, which follows the linear theory, will move much faster than a prograde vortex for $\ell/r_v \ll 1$. On other hand, when $\ell/r_v \sim 1$, the ratio between the radial velocities of a retrograde vortex and a prograde vortex will be about $2\pi^2$.

3. 2D Fluid Experiments with Magnetized Electron Plasmas

Many features of turbulent relaxation processes in 2D Euler fluids have been studied using electron plasmas confined in a Penning-Malmberg traps [1-4]. Conventional fluid experiments are difficult to manipulate and diagnose, and are subject to undesired viscous and boundary effects. With low viscosity, circular free-slip boundary conditions, simple manipulation technique, and accurate diagnostics, magnetized electron columns provide excellent opportunities to study 2D turbulence. However, few experimental studies have quantitatively measured 2D-vortex motion in a shearing background flow. So far, laboratory observations have been reported by Huang *et al.* [2], who measured only a single datum of the drift velocity of two holes down a vorticity gradient; and more recently by Kiwamoto *et al.* [4], who, on the contrary, only examined the dynamic behavior of electron clumps immersed in a background vorticity.

The experimental apparatus used at UCSD [2,3] is shown in Fig. 3. Electrons from a tungsten filament are contained inside a series of conducting cylinders of radius R_w = 3.5 cm enclosed in a vacuum chamber ($P \sim 10^{-10}$ torr) with uniform axial magnetic field B = 4 kG. The magnetic field provides radial confinement, and negative voltages (V_c = –80 V) applied on the two end cylinders provide axial confinement. A trapped electron column typically has maximum density $n_0 \sim 10^7$ cm^{-3}, radius $R_p \approx 2$ cm, axial length $L_p \approx 35$ cm, and electron thermal energy $T_e \approx 1$ eV. The rapid (~ 1 μs) axial bounce motion of individual electrons in comparison with the column bulk rotation time (~ 50 μs) effectively averages over any z variations. Together with small electron gyro-radius (~ 10 μm), it allows us to use the 2D $\mathbf{E}\times\mathbf{B}$ drift approximation [11,12] of the system macroscopic dynamics

$$\frac{\partial n}{\partial t} + \vec{v}\cdot\nabla n = 0\,,\quad \vec{v} = \hat{z}\times c\nabla\varphi/\boldsymbol{B}\,,\quad \nabla^2\varphi = 4\pi e n. \tag{9}$$

which is isomorphic to the 2D Euler equations [Eqs. (1)].

Comparing the drift-Poisson equations (9) to the Euler equations (1), we see that the vorticity $\zeta(r,\theta,t)$ is directly proportional to the electron density $n(r,\theta,t)$, i.e. $\zeta = 4\pi e c n/B$; and the stream function $\psi(r,\theta,t)$ is directly proportional to the electrostatic potential $\varphi(r,\theta,t)$, i.e. $\psi = c\varphi/B$; while nonzero $\mathrm{d}\varphi/\mathrm{d}r$ at the wall corresponds to the free-sleep boundary conditions. Therefore, the vorticity is simply advected in the incompressible flow with electron density, the streamlines conform to the equipotential surfaces, and vorticity measurements are equivalent to density measurements.

In the experiment, we first inject and trap a stable quiescent column with monotonically decreasing and cylindrically symmetric initial density profile $n_0(r)$. Then, we either create a narrow hole of radius $\rho_v \ll R_p$ at the center of electron column by temporarily decreasing the confinement voltage at one of the end cylinders and allowing electrons to escape from the trap; or combine the column with a small peripheral clump (which is prepared in adjacent trap). The column with either a clump or a hole then evolves for time t, after which the electron column is dumped axially onto a phosphor screen. The 2D density image $n(r,\theta,t)$ is recorded with a CCD camera, and $\zeta(r,\theta,t)$ is obtained

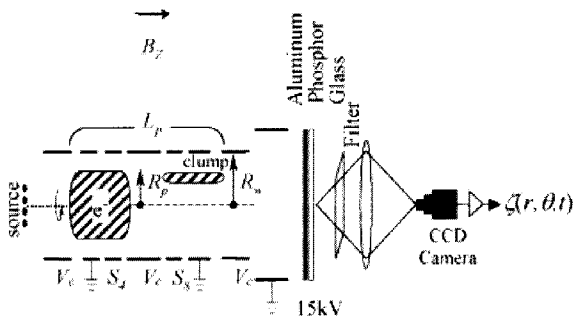

Fig. 3 Experimental apparatus (Penning-Malmberg trap) for 2D fluid experiments with magnetized electron plasmas.

directly. Although this imaging technique is destructive, the shot-to-shot variations for nearly identical initial conditions are small (< 1% in azimuthally averaged local density), so that the time evolution of a flow can be studied.

Figure 4 shows a typical example of background vorticity $\zeta_0(r)$ and rotation frequency $\Omega_0(r)$ profiles, as well as a profile. The chosen background vorticity distribution represents a large class, where plasma density decreases radially outward, and the radial derivatives of θ-averaged $\zeta_0(r)$ and $\Omega_0(r)$ vary slowly within $r < R_p$. Their characteristic values, used in the current experiments, were in the bands $50 \le \zeta_0' \le 500$ msec^{-1} cm^{-1} and $10 \le \Omega_0' \le 50$ msec^{-1} cm^{-1}, so that the condition of non-critical shear strength [9] $\zeta_0'/\Omega_0' > 1$ is always satisfied.

We can easily create clump (or hole) characterized by approximately "gaussian" density (vorticity) distribution with the maximum density n_v comparable to the background density scale n_0, and the characteristic radial extent $\rho_v \ge 0.1R_p \approx 0.2$ cm. In this case, the accessible region of vortex strengths is $\rho_v/R_p \le \ell/r_v \le (R_p/\rho_v)^{1/2}$, i.e., $0.1 \le \ell/r_v \le 3$. Thus, we can compare our experimental results to the linear analysis of vortex motion for $\ell/r_v \ll 1$, and also obtain results where the theory is invalid at $\ell/r_v \sim 1$.

Figure 5 shows the evolution of the measured vorticity distribution when either a clump or a hole is added to the initially symmetric background. The upper example [Fig. 5(a)] shows a retrograde clump climbing the vorticity gradient; whereas the lower sequence of images [Fig. 5(b)] shows a prograde hole moving down the gradient. Here, time is measured in units of the background's rotation period, $\tau \equiv 1/\Omega_0(r_v)$. Apparently, there are quite different time scales for these two series. The clump moves an order of magnitude faster than the hole.

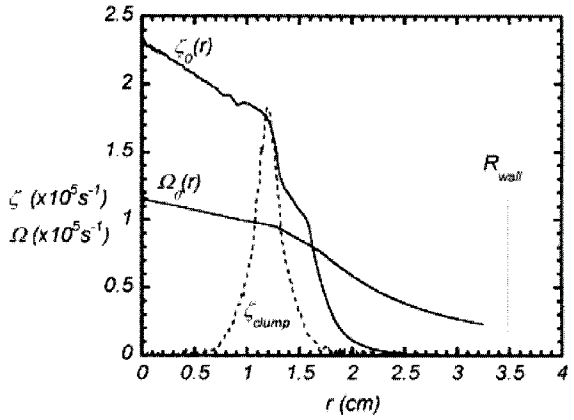

Fig. 4 Graph showing the radial cross-sectional distribution of the vorticity ζ_0 of a typical background flow, its rotation frequency Ω_0, as well as radial position and the vorticity of a generated clump ζ_{clump} (dashed line).

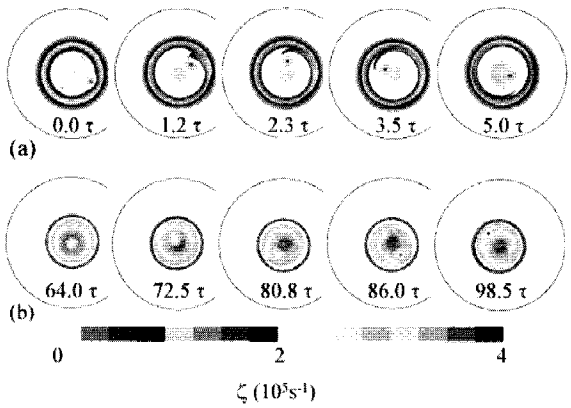

Fig. 5 The vorticity dynamics in two different experimental series: (a) motion of a retrograde clump, starting at the periphery, and (b) motion of a prograde hole, starting at the center. The repetitive vorticity grayscale is linear. The outer arcs indicate the wall radius R_{wall} = 3.5 cm. Time is measured in units of the vortex's rotation period, τ.

4. Analysis

Our experiments with retrograde clump placed initially at plasma column periphery ($r_v \approx R_p$) have shown that the clump rapidly ($t \ll \tau$) accelerates to an approximately constant radial velocity, and then spirals toward the center of background vorticity. The radial velocity of the clump increases with its circulation Γ_v and background vorticity gradient ζ_0', while it decreases as the local rotational shear Ω_0' intensifies. While the clump approaches close to the center of the background ($r_v \sim \rho_v$), within a time of a few orbiting periods it forms a dipolar structure, which is out of present consideration. Figure 6 shows a sequence of measured radial velocity points for retrograde clumps of different strength ℓ/r_v. In the plot, the radial velocity is normalized to $r_v^2\zeta_0'$ to emphasize the vortex strength characteristics of the motion. The plot also shows the results of linear computations [Eq. (4)] and VIC simulations [9]. There is a good agreement between experimental results, theory and VIC simulations in their intersection region, where $\ell/r_v \ll 1$. In this linear regime, the radial velocity scales as $dr_v/dt \propto \ell^2\zeta_0'$.

Moreover, the measured velocity shows the same trend in the transition region $\ell/r_v \sim 1$.

Experiments with prograde holes clearly show much smaller radial drift velocities. A centered hole is an (unstable) equilibrium, but it eventually moves off axis; in Fig. 5(b), this takes about 60τ. For comparison to theory, we consider the hole motion only when it is off-axis. When the hole has moved off center by a distance comparable to its size, it moves with a nearly constant radial velocity, and then spirals down the background vorticity gradient. As was the case for a retrograde clump, the hole's radial velocity scales as $dr_v/dt \propto \ell^2\zeta_0'$, but it is approximately 20 times slower. Unlike the clump motion, the hole needs tens of orbital periods to move radial distance of $R_p/2$ and reach the plasma column periphery.

Figure 6 shows the measured radial velocities for prograde holes of different strengths. The plot also shows the "mix-and-move" estimate [Eq. (8)] and data from VIC simulations, as well as the early measurements [2] of two small holes moving at the plasma column periphery. Again, like the case of retrograde clumps, one can see a quantitative agreement between the experiment, the "mix-and-move" estimate, and the VIC simulations for the prograde holes. We note again that the hole moves at much slower rate not because the hole has a negative vorticity, but because the hole is prograde with respect to the background shear flow in our experiments.

The experiments also show that a clump can get "stuck" in a region of a small vorticity gradient (Fig. 7). Here, the background vorticity has a shoulder with low local gradient ζ_0' and high rotational shear Ω_0', so that the mixing layer gets flattened before the vortex can move. Thus, the local mixing will not affect anymore the background vorticity distribution. Eq. (6) predicts that a vortex will not pass over a flat shoulder in the background vorticity distribution if $\Delta r/\ell \approx \zeta_0'/\Omega_0' < 1$. Figure 7 shows the background vorticity versus radius, and the radial position of the clump as a function of time (dots). The clump starts climbing the gradient and then stops moving radially at $r \approx 1.5$ cm, where the clump reaches the shoulder with clump-weighted $\zeta_0'/\Omega_0' \approx 1$, and then, in accordance to expectations, it settles on this shoulder to be eventually dispersed into the background.

Even more strikingly, the experiments show that the "wake" behind a moving clump can generate secondary holes and turbulence. Figure 8 shows the azimuthally asymmetric components of the perturbation

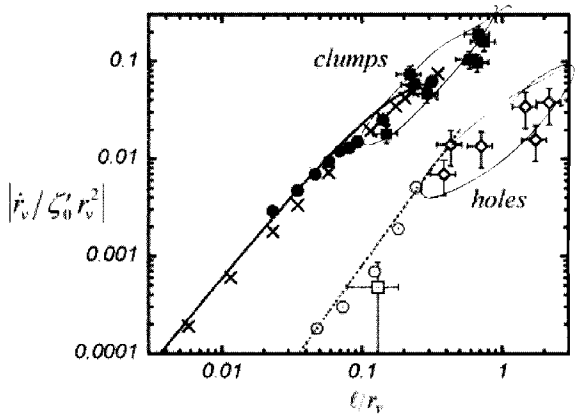

Fig. 6 Radial velocity dr_v/dt for retrograde clumps and prograde holes versus vortex strength ℓ/r_v in linear theory (solid curve, Eq. 4, $c = 0.43$), "mix-and-move" estimate (dashed line, Eq. 8), linear simulation (x's), VIC simulations (●'s and ○'s), and experiments (■'s and ◇'s). In the plot, dr_v/dt is normalized to $r_v^2\zeta_0'$ to emphasize this speed as a function of the vortex strength ℓ/r_v.

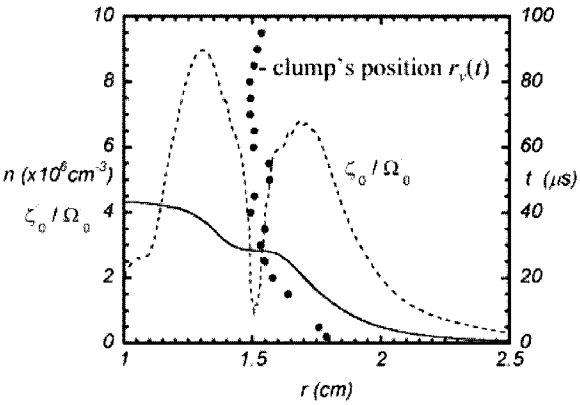

Fig. 7 Stagnation of the climbing clump motion on a flat shoulder of the background vorticity. Here, the gradient/shear strength parameter ζ_0'/Ω_0' is averaged over the clump scale. Note that only the periphery (1 cm < r < 2.5 cm) of the vorticity distribution is shown here.

to the background vorticity at different times during an ascending clump motion. The symmetric (θ-averaged) component of the background vorticity has been subtracted from the raw images, leaving only the asymmetric component. To conserve the total canonical angular momentum, the moving clump redistributes the background vorticity, which forms a spiral wake with low density at its inner side and increased density at its outer side. The wake gradually spirals outward [Fig.

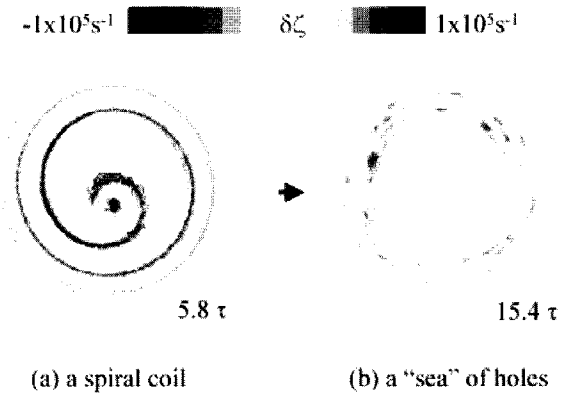

Fig. 8 Evolution of the background vorticity during a climbing clump motion. The images show only non-axisymmetric perturbations $\delta\zeta(r,\theta,t)$ of the θ-averaged background vorticity $\zeta_0(r,t)$.

8(a)], and eventually evolves through high m-modes of the Kelvin-Helmholtz instability into a set of small holes located near the plasma periphery [Fig. 8(b)]. Typically these holes are evenly spaced in θ and have close values of r_v. The slow drift of these holes out of the vorticity distribution controls the later stage of relaxation of this "turbulence" toward an ordered state. Descending spiral motion of prograde hole does not form such kind of wake due to fast and more thorough mixing of the background vorticity.

5. Conclusions

We have measured the radial drift velocities of finite-sized clumps and holes moving up and down vorticity gradient for a wide range of vortex strengths, background gradients, and background shear rates. All measurements are in quantitative agreement with recent theoretical analyses for weak vortices, and with numerical simulations.

Clumps and holes move in opposite directions and at substantially different rates. Both types of vortices mix the background vorticity and act to level its gradient. However, conservation of angular momentum dictates that clumps move up the background gradient, whereas holes move down the gradient. The rate of this motion is determined by whether the vortex is prograde or retrograde with respect to the local background shear: a prograde vortex moves at a much slower rate than a retrograde vortex. Sufficiently strong shear breaks down the "mix-and-move" model and can completely suppress this vortex motion on a gentle slope of a background vorticity.

A rapidly moving retrograde vortex leaves a spiral density wake, and instability of this wake eventually generates many long-lived holes, which contribute to the "turbulent" noise and slow down the relaxation rate.

Finally, we note that there is obvious discrepancy between the experimental dynamics and the point-like vortex theory computations when the vortex of real finite size gets close to the background center, where it forms a dipolar structure and exhibits a slowly decaying oscillatory motion. This finite scale behavior merits further study.

Acknowledgment

This work was supported by National Science Foundation Grant PHY-987699.

References

[1] D.L. Eggleston, Phys. Plasmas **1**, 3850 (1994).
[2] X.-P. Huang, K.S. Fine and C.F. Driscoll, Phys. Rev. Lett. **74**, 4424 (1995).
[3] K.S. Fine *et al.*, Phys. Rev. Lett. **75**, 3277 (1995).
[4] Y. Kiwamoto *et al.*, Phys. Rev. Lett. **85**, 3173 (2000).
[5] C.G. Rossby, J. Mar. Res. **7**, 175 (1948).
[6] R.K. Smith and W. Ulrich, Q. J. R. Meteorol. Soc. **119**, 207 (1993).
[7] G.M. Reznik and W.K. Dewar, J. Fliud. Mech. **269**, 301 (1994).
[8] W.H. Shubert *et al.*, J. Atmos. Sci. **56**, 1197 (1999).
[9] D.A. Schecter and D.H.E. Dubin, Phys. Rev. Lett. **83**, 2191 (1999).
[10] T.H. Dupree, Phys. Fluids **26**, 2460 (1983).
[11] R.J. Briggs, J.D. Daugherty and R.H. Levy, Phys. Fluids **13**, 421 (1970); R.H. Levy, Phys. Fluids **11**, 920 (1968).
[12] C.F. Driscoll and K.S. Fine, Phys. Fluids B **2**, 1359 (1990).